THIRTEENTH EUROPEAN ROTORCRAFT FORUM

Paper No. 6 73

EFFECTS OF DIFFERENCE IN INDUCED VELOCITY DISTRIBUTION ON THE HELICOPTER MOTION

Yoshinori OKUNO, Akira AZUMA and Keiji KAWACHI

Institute of Interdisciplinary Research
Faculty of Engineering, The University of Tokyo
4-6-1, Komaba, Meguro-ku,
Tokyo, 146 Japan

September 8-11,1987

ARLES,FRANCE

ASSOCIATION AERONAUTIQUE ET ASTRONAUTIQUE DE FRANCE

EFFECTS OF DIFFERENCE IN INDUCED VELOCITY DISTRIBUTION ON THE HELICOPTER MOTION

Yoshinori OKUNO, Akira AZUMA and Keiji KAWACHI

The University of Tokyo
Tokyo, Japan

ABSTRACT

Limits or allowable range of application of the simple momentum theory is made clear in comparison with the local momentum theory,[1],[2].

As far as concerning the helicopter motion in high μ flight, there is no difference in the results calculated by the above two theories. However, for the helicopter motion in low μ flight and for the blade deflections in either low or high μ flight, some discrepancies can be observed in the results based on the above two theories, because of a difference in the induced velocity distribution.

1. Introduction

Every blade of helicopter rotor is operating under influences of induced velocity distribution generated by preceding blades and of the blade motion coupled with the helicopter motion. As far as concerning an isolated rotor motion, the vortex theory gives a precise information on the induced velocity distribution on the rotor disc. However, if the rotor motion is coupled with the helicopter motion, then the calculation of the induced velocity on the rotor blades is not easy because of the complexity, divergent tendency and long computation time in the calculation.

Thus, in the actual calculations by combining with the blade element theory, the simple momentum theory (SMT) which assumes a constant induced velocity distribution on the rotor disc is very effective to give simply analytic solutions on the blade motion and the helicopter motion. However, this method of calculation occasionally brings erroneous conclusions on the stress analysis of the rotor blade and the resulted helicopter motion, specifically in low flight speed.

A purpose of this paper is, therefore, to calculate more precisely the spanwise and timewise change of the induced velocity distribution of a helicopter rotor operating in unsteady conditions than the momentum theory by using the local momentum theory (LMT). And another purpose is to compare the results obtained by the above two methods, the SMT and the LMT, and to make clear the limit or allowable range of application of the SMT to the actual problems.

2. Equations of Motion

Let us consider a helicopter motion with six-degrees of freedom disturbed by external forces and moments which are calculated by either the SMT or the LMT.

(1) Body Motion

$$\dot{u}=F_X/m-qw+rv \qquad -(1a)$$

$$\dot{v}=F_Y/m-ru+pw \qquad -(1b)$$

$$\dot{w}=F_Z/m-pv+qu \qquad -(1c)$$

$$\dot{p}=[\{M_X-(I_Z-I_Y)qr+qpJ_{ZX}\}I_Z+\{M_Z-(I_Y-I_X)qp-qrJ_{ZX}\}J_{ZX}] /(I_XI_Z-J_{ZX}^2) \qquad -(2a)$$

$$\dot{q}=\{M_Y-(I_X-I_Z)pr-(p^2-r^2)J_{ZX}\}/I_Y \qquad -(2b)$$

$$\dot{r}=[\{M_Z-(I_Y-I_X)qp-qrJ_{ZX}\}I_X+\{M_X-(I_Z-I_Y)qr+qpJ_{ZX}\}J_{ZX}] /(I_XI_Z-J_{ZX}^2) \qquad -(2c)$$

(2) Blade Motion

flapping

$$I_\beta\ddot{\beta}+K_{\dot{\beta}}\dot{\beta}+M_\beta\Omega^2\beta+K_\beta(\beta-\overline{\beta_0})-\int_{r_c}^{R}l(r-r_\beta)dr +m_\beta rg-2(p_s\cos\psi-q_s\sin\psi)M_\beta\Omega=0 \qquad -(3a)$$

lead-lag

$$I_\zeta\ddot{\zeta}+K_{\dot{\zeta}}\dot{\zeta}+M_\zeta\Omega^2\zeta+K_\zeta(\zeta-\overline{\zeta_0})-\int_{r_c}^{R}d(r-r_\zeta)dr -2\int_{r_\beta}^{R}(r-r_\zeta)(r-r_\beta)\Omega\beta\dot{\beta}dm=0 \qquad -(3b)$$

(3) Blade deflection

flatwise

$$[\{EI_y+(EI_z-EI_y)\sin^2\theta\}w'' +(EI_z-EI_y)(v''\sin2\theta/2+\phi v''\cos2\theta+\phi w''\sin2\theta)]'' -(Tw')'+m(\ddot{w}+e\ddot{\phi}) =F_{az}-m(g+e\ddot{\theta}-e\Omega^2\theta) \qquad -(4a)$$

chordwise

$$[(EI_z-(EI_z-EI_y)\sin^2\theta)v''$$
$$+(EI_z-EI_y)(w''\sin 2\theta/2-\phi v''\sin 2\theta+\phi w''\cos 2\theta)]''$$
$$-(Tv')'+m[\ddot{v}-e\theta\ddot{\phi}-\Omega^2(v-e\theta\phi)]$$
$$=F_{ay}+m[2\Omega u+2e\Omega(\dot{v}'+\theta\dot{w}')+e\theta\ddot{\theta}+\Omega^2(e_0+2e)] \qquad -(4b)$$

torsion

$$-[(GJ+Tk_A^2)\phi']'+(EI_z-EI_y)[(w''^2-v''^2)\sin 2\theta/2+v''w''\cos 2\theta]$$
$$+mk^2(\ddot{\phi}+\Omega^2\phi)+me[\ddot{w}-\theta\ddot{v}+\theta\Omega^2 v+e\Omega^2\phi+r\Omega^2(w'-\theta v')]$$
$$=M_{ax}-m[eg+k^2(\ddot{\theta}+\Omega^2\theta+2\Omega\theta\dot{v}')+e\theta(e_0\Omega^2-2\Omega\dot{u})] \qquad -(4c)$$

(4) Inflow in the Simple Momentum Theory

steady

$$\lambda = \mu\tan i + C_T/2\sqrt{\lambda^2+\mu^2} \qquad -(5a)$$

unsteady

$$\tau\dot{\lambda}+\lambda = L\,C_T \qquad -(5b)$$

3. Trim Analysis

By selecting adequate control inputs such as collective pitch control of main and tail rotors, and longitudinal and lateral cyclic pitch controls, a trimmed state of rotor and helicopter motion can be obtained for a given set of advance ratio and flight path angle of a helicopter, detailed dimensions of which are given in Table 1.

For the calculation of the induced velocity, three methods of computation coupled with the blade element theory are considered here;

(i) simple momentum theory (SMT),

(ii) local momentum theory (LMT).

For the calculation of airloading along the blade span and the flapping motion of the blade, two methods are considered;

(a) Under assumptions that the blade is infinitely rigid except a part of equivalent flapping hinge and the flapping motion is comprised of the first harmonic motion, in addition to the constant induced velocity given by the SMT, the airloading and the flapping motion can be analytically obtained

(b) By disregarding the above assumptions the airloading and the blade motions are calculated by the Runge-Kutta method.

Shown in Fig.1 is a set of trimmed quantities calculated by three methods; combination of (i)&(a), (i)&(b), and (ii)&(b), for a hingeless-rotor helicopter flying with various flight speeds in comparison with experimental data. It can be seen that there is not any appreciable discrepancy in these quantities among the above three methods and the experimental data.

However, as shown in Fig.2 and Fig.3, there are some differences in the angle of attack distribution of the blade over the rotor disc between two methods, (i)&(b) and (ii)&(b) or between the SMT and the LMT, specifically for low μ flight.

4. Control Response

Shown in Fig.4 and 5 are control responses by an impulsive input of -0.75 degrees for one second (-0.75 deg x 1 sec) in longitudinal cyclic pitch for the helicopter flying with trimmed advance ratio of μ=0.05 and μ=0.20 respectively.

As seen from Fig.2 appreciable differences are observed in almost all quantities for the low μ flight. Specifically, the rolling motion, which is typically observed in the hingeless-rotor helicopter for the longitudinal cyclic pitch input, is stressed more in the method of (i)&(b) than in the method of (ii)&(b). However, as seen from Fig.3 in the high μ flight there are no differences for all quantities between the two methods of calculation because the effect of the induced velocity on the angle of attack distribution is small.

5. Gust Response

Shown in Fig.6 through 8 are gust responses for sinusoidal vertical gusts in frozen state with the frequency of 2.0 and 0.5 Hz for the helicopter flying with advance ratio of μ=0.05 and 0.20.

Like the control response, the difference of the method of calculation between (i)&(b) and (ii)&(b) or the difference of the induced velocity distribution, is appreciable in the low μ flight as seen from Fig.6 and 7 and in the high frequency gust as seen from Fig.6 and 8. It can further be observed that the method of (i)&(b) tends to overestimate the hub moment in the low μ flight.

6. Consideration on the Dynamic Inflow

In the calculation of so called "dynamic inflow", [3],[4], the induced velocity given by equation (5b) is considered to be related to the rotor disc but not related to the blade, and the development of the induced velocity has a time lag due to the inertia effect of the added mass related to the rotor motion.

Therefore in the gust of small wavelength over the rotor radius such as $\lambda/R \leqq 1.0$ the above concept can not be applied.

For large wavelength over the rotor radius $\lambda/R >> 1.0$ the dynamic inflow is effective only for high frequency or high μ flight because the frequency is proportional to the flight speed over the wavelength. However, in the high μ flight the effect of the induced velocity on the airloading is not predominant.

In the control response, however, the control input with high frequency for the helicopter flying with low μ is one of subjects of the dynamic inflow.

7. Blade Deflection

The equations of blade deflections, equation (4a)~(4c), are solved by the Holzer-Myklestad method, [5],[6].

Shown in Fig.9a~d are induced velocity, airloading, flatwise bending moment, flatwise deflection, as a function of the spanwise distance, for the hingeless-rotor helicopter flying with $\mu=0.20$. Some discrepancies in the above quantities can be observed between the method of (i)&(b) and (ii)&(b) even in this advance ratio of $\mu=0.20$, at which there is little difference in the helicopter motion between the two methods as stated in the previous sections.

8. Dynamic Analysis by Means of Linearized Equations

By introducing a perturbed motion, the following linearized equations of motion can be derived;

$$
\begin{bmatrix} m\mu_X \\ m\mu_Y \\ I_Y q \\ \Theta \\ m\mu_Y \\ I_X p \\ I_Z r \\ \Phi \end{bmatrix} =
\begin{bmatrix}
X_{\mu_X} & X_{\mu_Z} & X_q - m\mu_{Zo} & X_\Theta & X_{\mu_Y} & X_p & X_r + m\mu_{Yo} & X_\Phi \\
Z_{\mu_X} & Z_{\mu_Z} & Z_q - m\mu_{Xo} & Z_\Theta & Z_{\mu_Y} & Z_p - m\mu_{Yo} & Z_r & Z_\Phi \\
M_{\mu_X} & M_{\mu_Z} & M_q & 0 & M_{\mu_Y} & M_p & M_r & 0 \\
0 & 0 & 1 & 0 & 0 & 0 & 0 & 0 \\
Y_{\mu_X} & Y_{\mu_Z} & Y_q & Y_\Theta & Y_{\mu_Y} & Y_p + m\mu_{Xo} & Y_r - m\mu_{Xo} & Y_\Phi \\
L_{\mu_X} & L_{\mu_Z} & L_q & 0 & L_{\mu_Y} & L_p & L_r & 0 \\
N_{\mu_X} & N_{\mu_Z} & N_q & 0 & N_{\mu_Y} & N_p & N_r & 0 \\
0 & 0 & 0 & 0 & 0 & 1 & 0 & 0
\end{bmatrix}
\cdot
\begin{bmatrix} \mu_X \\ \mu_Z \\ q \\ \Theta \\ \mu_Y \\ p \\ r \\ \Phi \end{bmatrix}
\qquad -(6)
$$

The external forces and moments $F=(X,Y,Z,L,M,N)^T$ generated by the main rotor, the tail rotor, and the fuselage are expanded by the Taylor series as follows;

$$\frac{dF}{d\theta} = \frac{dC_R}{d\theta} + \frac{dC_T}{d\theta} + \frac{dC_B}{d\theta} \qquad -(7a)$$

$$\frac{dF}{d\mu} = \frac{dC_R}{d\mu} + \frac{dC_T}{d\mu} + \frac{dC_B}{d\mu} \qquad -(7b)$$

$$\frac{dF}{d\varepsilon} = \frac{dC_R}{d\varepsilon} + \frac{dC_T}{d\varepsilon} + \frac{dC_B}{d\varepsilon} \qquad -(7c)$$

$$\frac{dF}{dE} = \frac{dC_G}{dE} \qquad -(7d)$$

$$\frac{dC_R}{d\theta} = \left(\frac{\partial}{\partial\theta} + \frac{d\beta}{d\theta}\frac{\partial}{\partial\beta} + \frac{d\lambda}{d\theta}\frac{\partial}{\partial\lambda}\right) C_R$$

$$= \left\{\frac{\partial}{\partial\theta} + \left(\frac{\partial}{\partial\theta} + \frac{d\lambda}{d\theta}\frac{\partial}{\partial\lambda}\right)\beta\frac{\partial}{\partial\beta} + \frac{d\lambda}{d\theta}\frac{\partial}{\partial\lambda}\right\} C_R \qquad -(8a)$$

$$\frac{dC_R}{d\mu} = \left(\frac{d\mu}{d\mu}\frac{\partial}{\partial\mu} + \frac{d\lambda}{d\mu}\frac{\partial}{\partial\lambda}\right) C_R$$

$$= \left\{\frac{d\mu}{d\mu}\left(\frac{\partial}{\partial\mu} + \frac{d\beta}{d\mu}\frac{\partial}{\partial\beta}\right) + \frac{d\lambda}{d\mu}\left(\frac{\partial}{\partial\lambda} + \frac{d\beta}{d\lambda}\frac{\partial}{\partial\beta}\right)\right\} C_R \qquad -(8b)$$

$$\frac{dC_R}{d\varepsilon} = \left(\frac{\partial}{\partial\varepsilon} + \frac{d\beta}{d\varepsilon}\frac{\partial}{\partial\beta} + \frac{d\mu}{d\varepsilon}\frac{\partial}{\partial\mu} + \frac{d\lambda}{d\varepsilon}\frac{\partial}{\partial\lambda}\right) C_R$$

$$= \left\{\frac{\partial}{\partial\varepsilon} + \left(\frac{\partial}{\partial\varepsilon} + \frac{d\mu}{d\varepsilon}\frac{\partial}{\partial\mu} + \frac{d\lambda}{d\varepsilon}\frac{\partial}{\partial\lambda}\right)\beta\frac{\partial}{\partial\beta} + \frac{d\mu}{d\varepsilon}\frac{\partial}{\partial\mu} + \frac{d\lambda}{d\varepsilon}\frac{\partial}{\partial\lambda}\right\} C_R \qquad -(8c)$$

where the advanced ratio μ, the inflow ratio λ, and the flapping angles β are considered to be intermediate variables for other independent variables and for themselves. The derivatives specified in equation (7a)~(7d) are, therefore, given by the analytic expressions of the total derivatives which are also consisted of the partial derivatives as given by equations (8a)~(8c).

Shown in Fig.10 and 11 are control responses for lateral cyclic and longitudinal cyclic pitch inputs respectively in the helicopter flying with μ=0.20. By applying two methods of calculation, (i)&(a) and (ii)&(b), it can be revealed that as seen from Fig.10 there is no distinctive difference between the two methods within a short period, but as seen from Fig.11 the damping of oscillation in the method of (i)&(a) is much smaller than the expected values as given by the method of (ii)&(b).

Fig.12 shows roots of the characteristic equation of the helicopter motion in a complex plane. The method of (i)&(a) gives roots of less damping than those given by the method of (ii)&(b).

Fig.13a~e show mode ratios based on the pitching angle Θ for the longitudinal motion and the rolling angle Φ for the lateral motion. The difference between the two methods of calculation appears in the coupling motion, specifically in the phase angle rather than the amplitude.

9. Conclusion

Three methods of calculation, essentially based on either the simple momentum theory or the local momentum theory for the induced velocity distribution, and combined with either the analytic method or computational method for the helicopter and blade motions, are applied to get control responses and gust responses of a hingeless-rotor helicopter.

There are some discrepancies in the helicopter motions given by two methods based on the SMT and the LMT in the low μ flight but not in the high μ flight. However some differences can be observed in the bending moment and deflections of the blade even in the high μ flight.

Analytic method based on the linearized equations of motion gives appropriate solutions for the helicopter motion but the dampings of the motion are underestimated in comparison with the method of the LMT and the numerical integration. For the coupling motion, the above analytic method gives some phase difference from the method of LMT.

References

[1] A. Azuma and K. Kawachi, Local Momentum Theory and Its Application to the Rotary Wing. J. Aircraft 16, 6-14, 1979; also AIAA Paper 75-865, 1976.

[2] S. Saito, A. Azuma, K. Kawachi, and Y. Okuno, Study of the Dynamic Responses of Helicopters to a Large Airplane Wake, 12th European Rotorcraft Forum, Paper No.42, Sep. 1986.

[3] P.J. Carpenter and B.Fridovitch, Effect of Rapid Blade Pitch Increase on the Thrust and Induced Velocity Response of a Full Scale Helicopter Rotor, NACA TN-3044, Nov. 1953.

[4] D.M. Pitt and D.A. Peters, Theoretical Prediction of Dynamic-Inflow Derivatives, Vertica Vol.5., 1981.

[5] N.O. Myklestad, A New Method of Calculation Natural Modes of Uncoupled Bending Vibration of an Airplane Wings and Other Types of Beams, J. Aeronautical Science, Apr. 1944.

[6] N.O. Myklestad, Fundamentals of Vibration Analysis, McGraw-Hill Book Company Inc., N.Y., 1944.

NOMENCLATURE

$C_R=(C_T, C_H, C_Y, C_Q, C_L, C_M)$	nondimensional forces and moments of rotor
$E=(\Phi, \Theta, \Psi)$	euler angle of the helicopter
EI	bending stiffness of blade
e	distance between mass and elastic axis
$F=(F_X, F_Y, F_Z, M_X, M_Y, M_Z)$	external forces and moments
GJ	torsional stiffness of blade
I_X, I_Y, I_Z	moments of inertia of the helicopter
I_β	moment of inertia about flapping hinge
I_ζ	moment of inertia about lead-lag hinge
i	inflow angle
J_{ZX}	product of inertia of the helicopter
K_β	flapping spring stiffness
K_β	flapping damping constant
K_ζ	lead-lag spring stiffness
K_ζ	lead-lag damping constant
k_ζ	polar radius of gyration per unit span
M_β	mass moment about flapping hinge
M_ζ	mass moment about lead-lag hinge
m_ζ	mass of the blade about flapping hinge
m_β	mass of the blade about lead-lag hinge
R_ζ	blade radius
r_C	blade cut-off radius
r_β	flapping hinge offset
r_ζ	lead-lag hinge offset
T_ζ	$=\Omega^2\int_r^R mrdr$ (in equation(4))
u, v, w	flight speed in body coordinate system
	displacement of elastic axis of the blade
$\beta=(\beta o, \beta s, \beta c)$	blade flap angle
β	flapping angle, angle of side slip
$\overline{\beta o}$	pre-coning angle
$\varepsilon=(p, q, r)$	angular velocity
ζ	lead-lag angle
$\overline{\zeta o}$	pre-lag angle
$\theta=(\theta o, \theta s, \theta c)$	blade pitch angle
λ	inflow ratio
μ	advance ratio
$\mu=(\mu_X, \mu_Y, \mu_Z)$	nondimensional flight speed
τ	time constant
ϕ	elastic torsional deformation of the blade
ψ	azimuth angle
Ω	rotor rotational speed
$()_A$	quantity concerning airloads
$()_B$	quantity concerning fuselage (including tail planes)
$()_G$	quantity concerning gravity
$()_R$	quantity concerning main rotor
$()_S$	quantity concerning rotor shaft
$()_T$	quantity concerning tail rotor
$\dot{()}$	time derivation
$()'$	spanwise derivation

Table 1 Dimensions of a hingeless-rotor helicopter

Gross mass, m(kg)	2,850
Moment of inertia of body, I_X(kgm²)	2,380
I_Y(kgm²)	7,314
I_Z(kgm²)	5,560
J_{ZX}(kgm²)	1,057
For Main Rotor	
Rotor radius, R(m)	5.5
Number of blades, b	4
Blade chord, c(m)	0.32
Blade twist, θ_t(deg)	-8.0
Rotor rotational spee, Ω(rad/s)	40.15
Blade mass, m_β(kg)	31.95
Moment of inertia of blade, I_β(kgm²)	212.66
Inclination of rotor shaft, i_s(deg)	5.0
Equivalent hinge offset, x_β	0.129
x_ζ	0.145
Equivalent hinge stiffness, k_β(Nm/rad)	149.0
k_ζ(Nm/rad)	816.0
Preconing angle, β(deg)	2.5
Longitudinal position, l_R(m)	-0.135
Hight of main rotor, h_R(m)	1.50
For Tail Rotor	
Rotor radius, R_T(m)	0.95
Number of blades, b_T	2
Blade chord, c_T(m)	0.18
Blade twist, θt_T(deg)	0.0
Rotor rotational speed, Ω(rad/s)	227.2
Blade mass, m_T	0.94
Moment of inertia of blade, I_{β_T}(kgm²)	0.28
δ_3 hinge, δ_3(deg)	45.0
Longitudinal position, l_T(m)	6.48
Hight of tail rotor, h_T(m)	1.64
For Fuselage	
Area, S_F(m²)	3.68
Drag coefficient, C_{D_F}	0.315
For Horizontal Tail	
Wing area, S_H(m²)	1.0
Span, b_H(m)	2.5
Chord, c_H(m)	0.4
Aspect ratio, AR_H	2.17
Longitudinal position, l_H(m)	5.06
Hight of horizontal tail, h_H(m)	0.62
Angle of incidence, i_H(deg)	-1.5
For Vertical Tail	
Wing area, s_V(m²)	2.24
Span, b_V(m)	1.28
Chord, c_V(m)	1.75
Aspect ratio, AR_V	0.73
Longitudinal position, l_V(m)	5.27
Hight of vertical tail, h_V(m)	0.22
Angle of incidence, i_V(deg)	-7.0

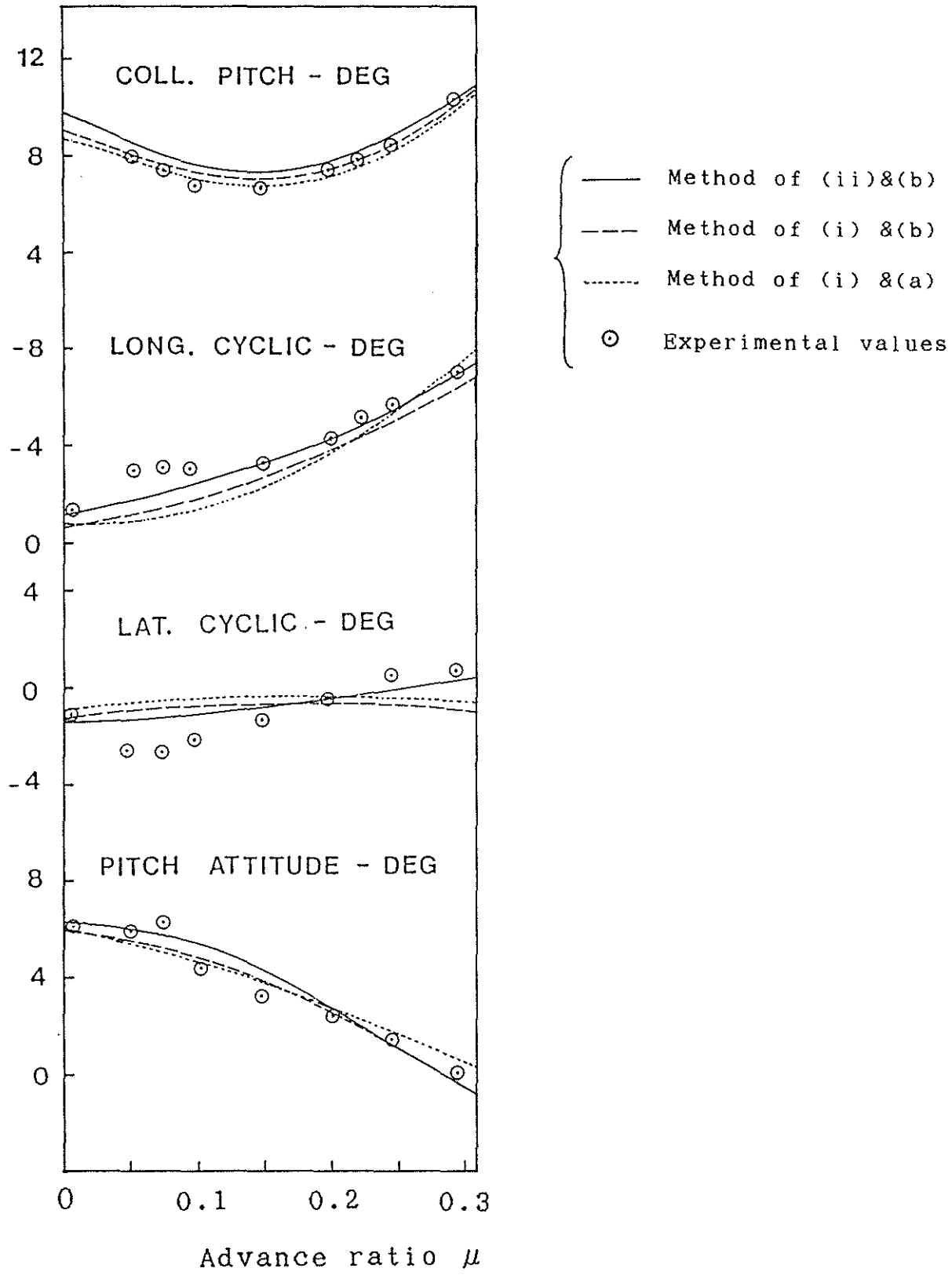

Figure 1 Trim analysis of the helicopter

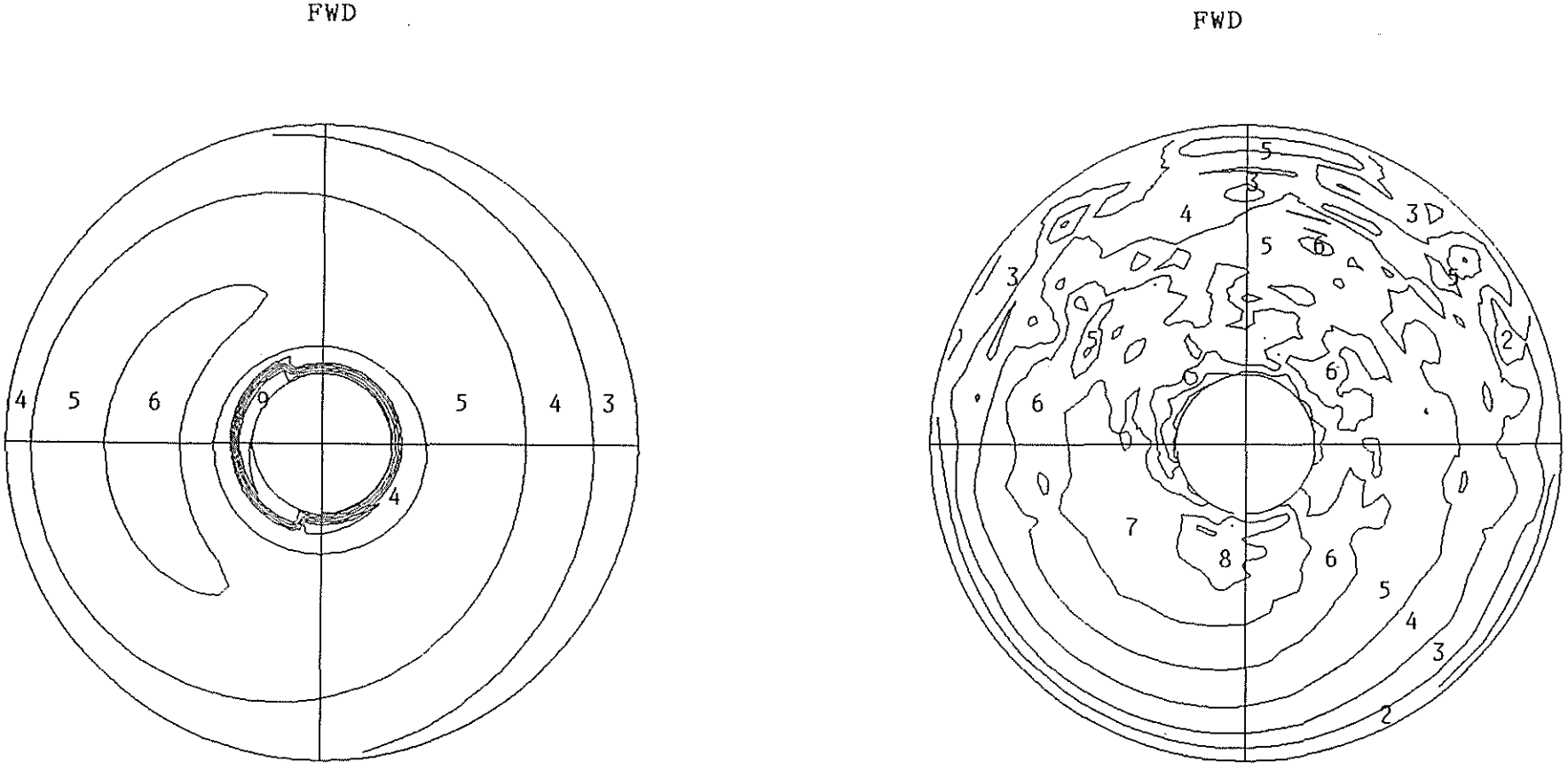

(a) Method of (i) &(b)

(b) Method of (ii)&(b)

Figure 2 Angle of attack distributions on the rotor blade flying with advance ratio of μ=0.05

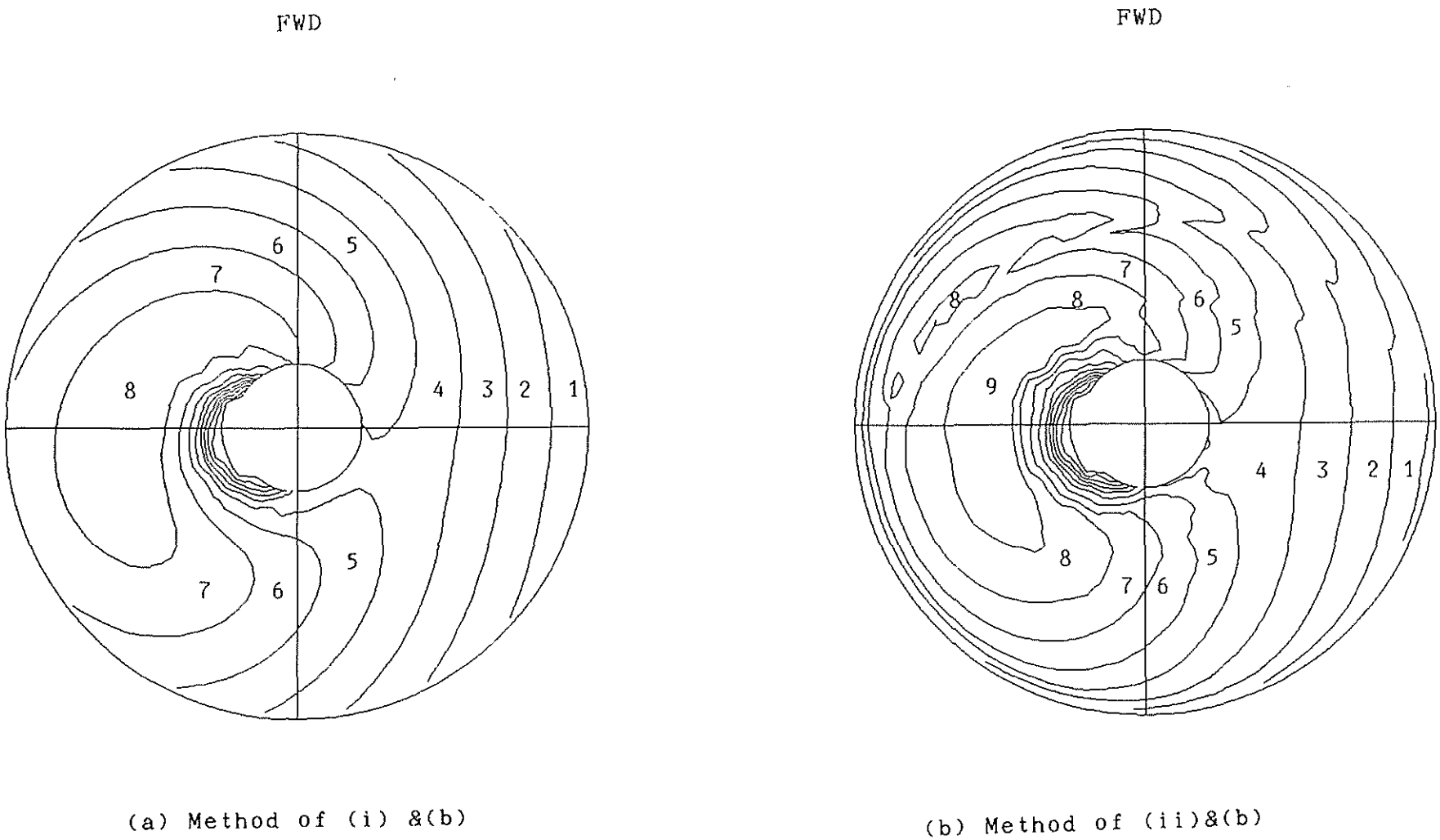

(a) Method of (i) &(b)

(b) Method of (ii)&(b)

Figure 3 Angle of attack distributions of the helicopter flying with advance ratio of μ=0.20

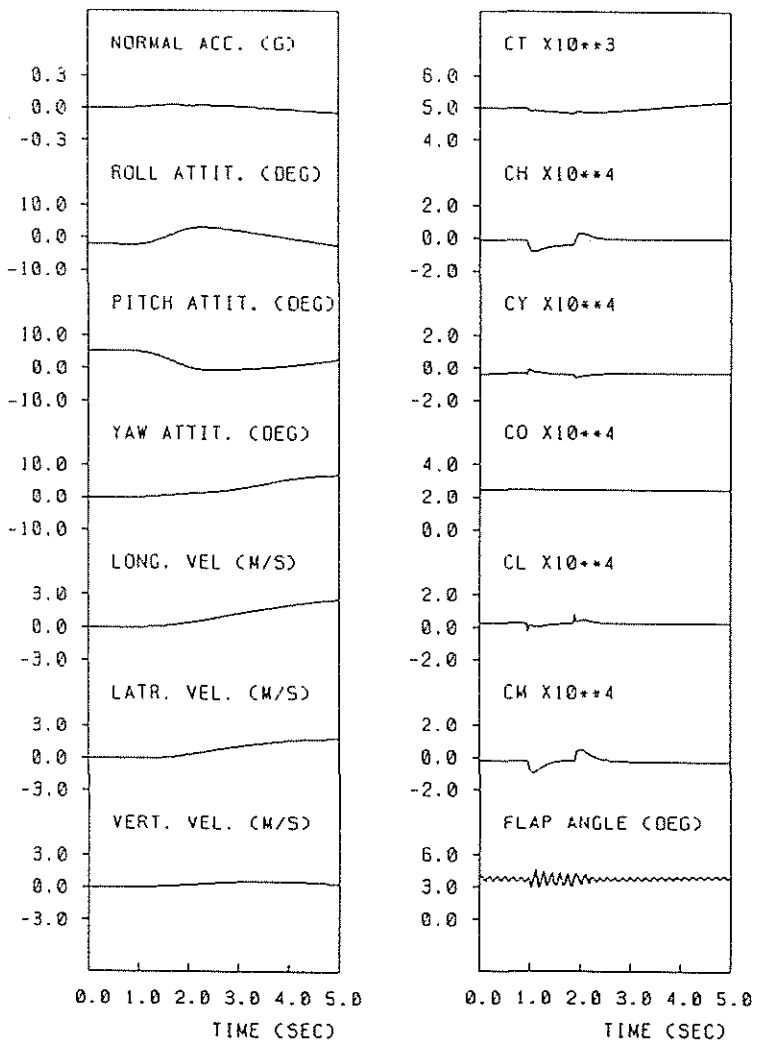

(a) Method of (i) &(b)

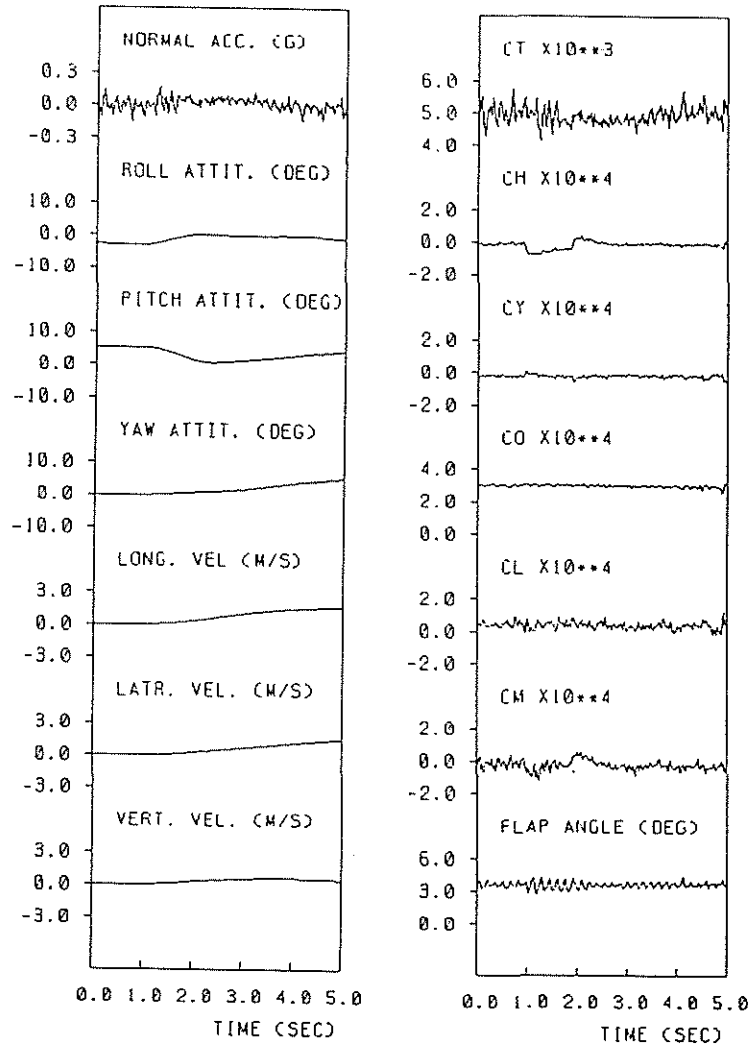

(b) Method of (ii)&(b)

Figure 4 Control responses of the helicopter flying with advance ratio of μ=0.05 for an impulsive input ($\Delta\theta$s=-0.75° and Δt=1s)

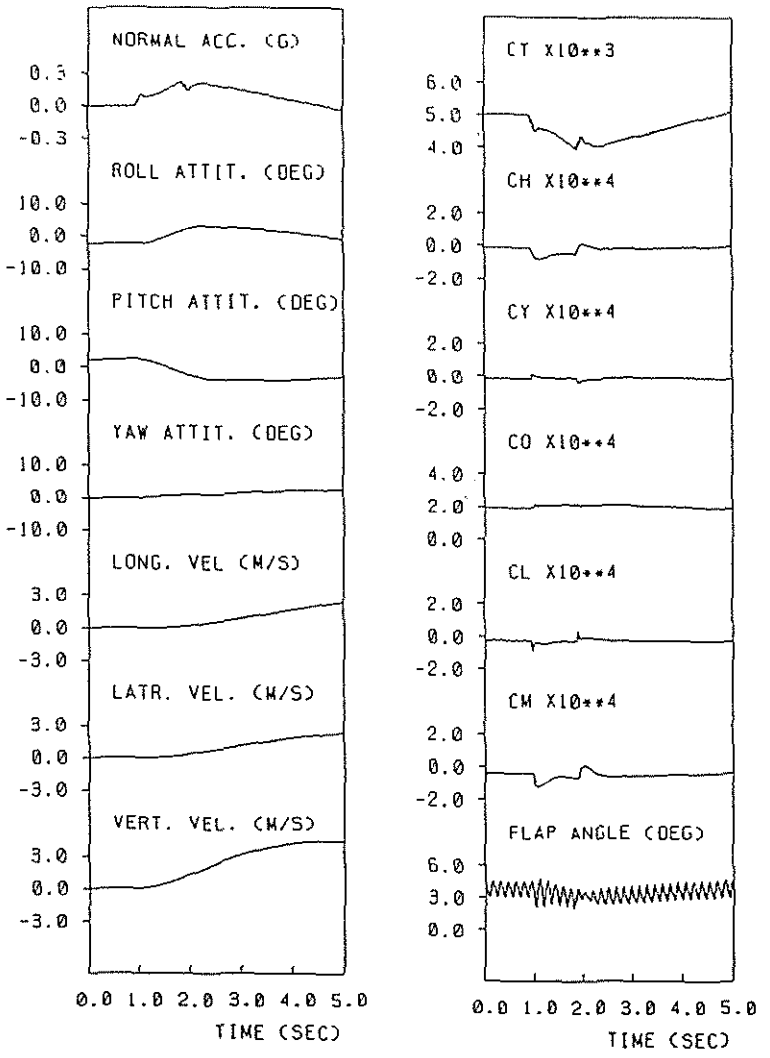

(a) Method of (i) &(b)

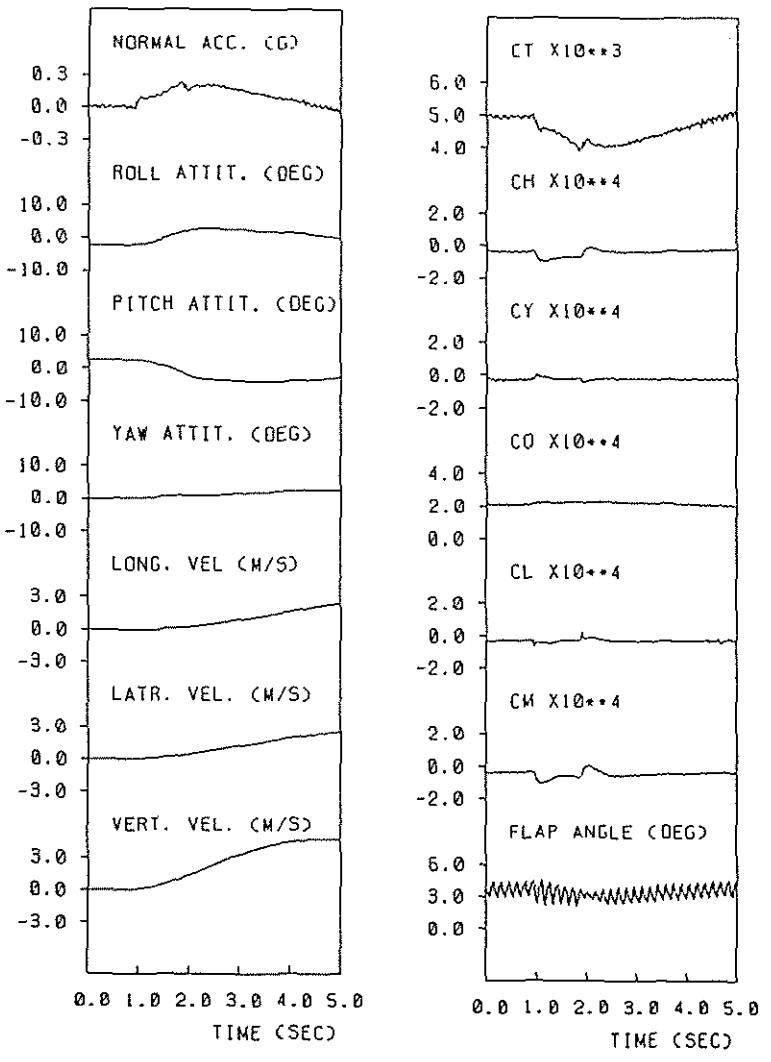

(b) Method of (ii)&(b)

Figure 5 Control responses of the helicopter flying with advance ratio of μ=0.20 for an impulsive input ($\Delta\theta$s=-0.75° and Δt=1s)

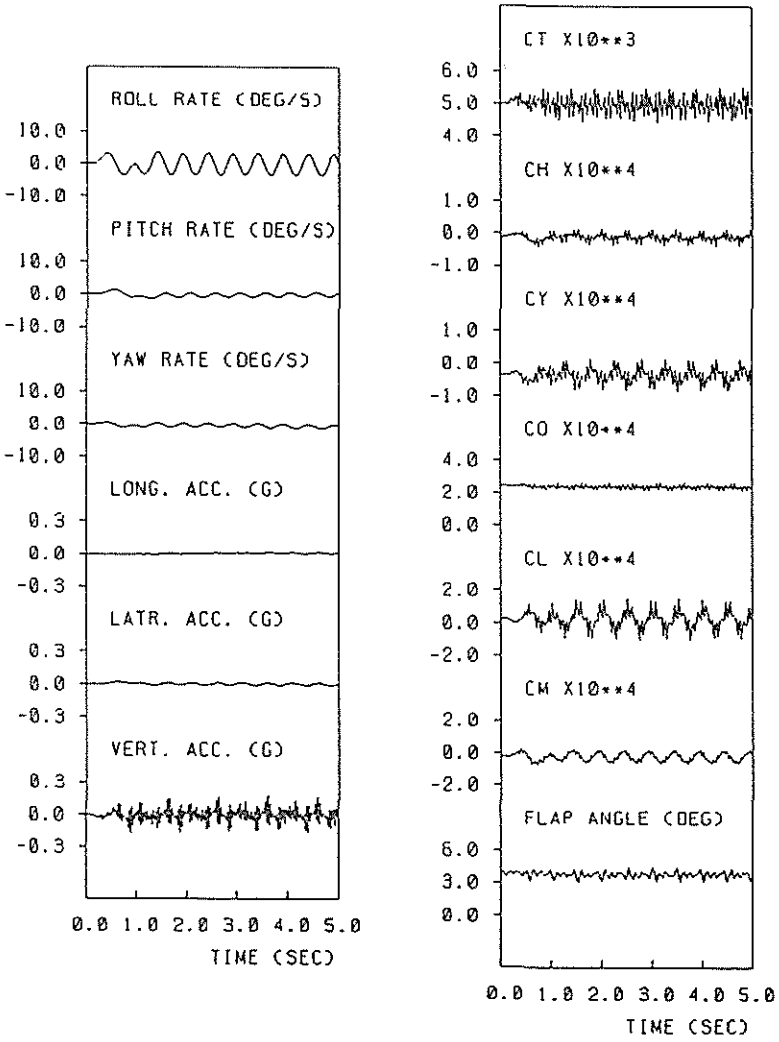

(a) Method of (i) &(b)

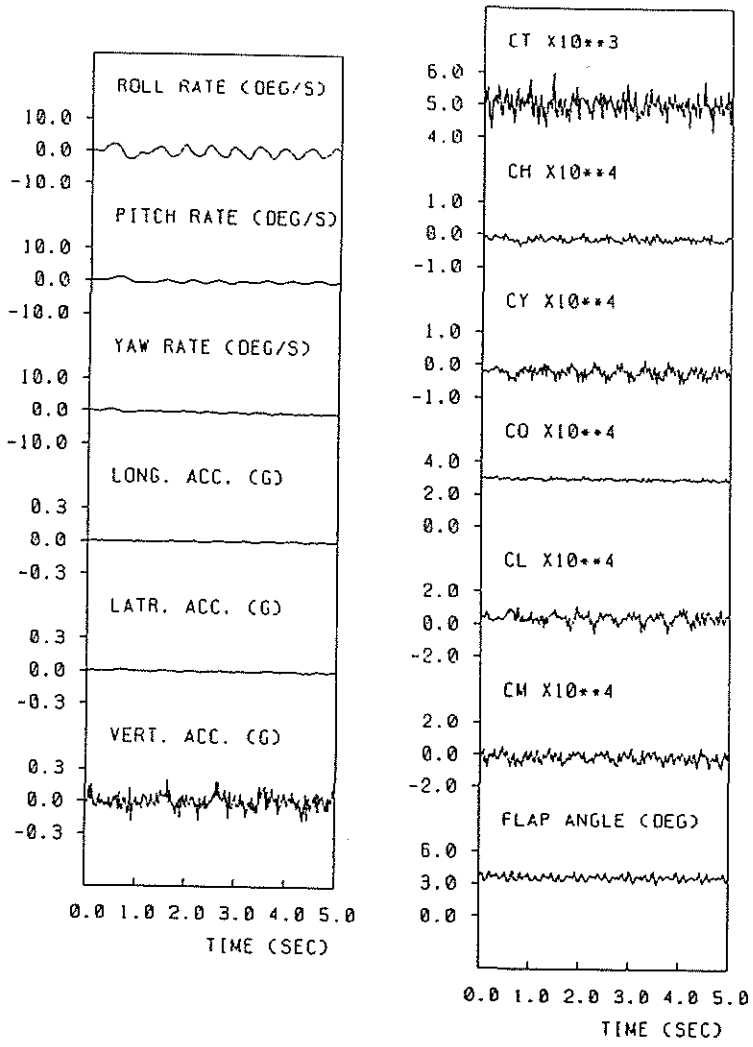

(b) Method of (ii)&(b)

Figure 6 Gust responses of the helicopter flying with advance ratio of μ=0.05 for a sinusoidal gust (amplitude of 3m/s and frequency of 2Hz)

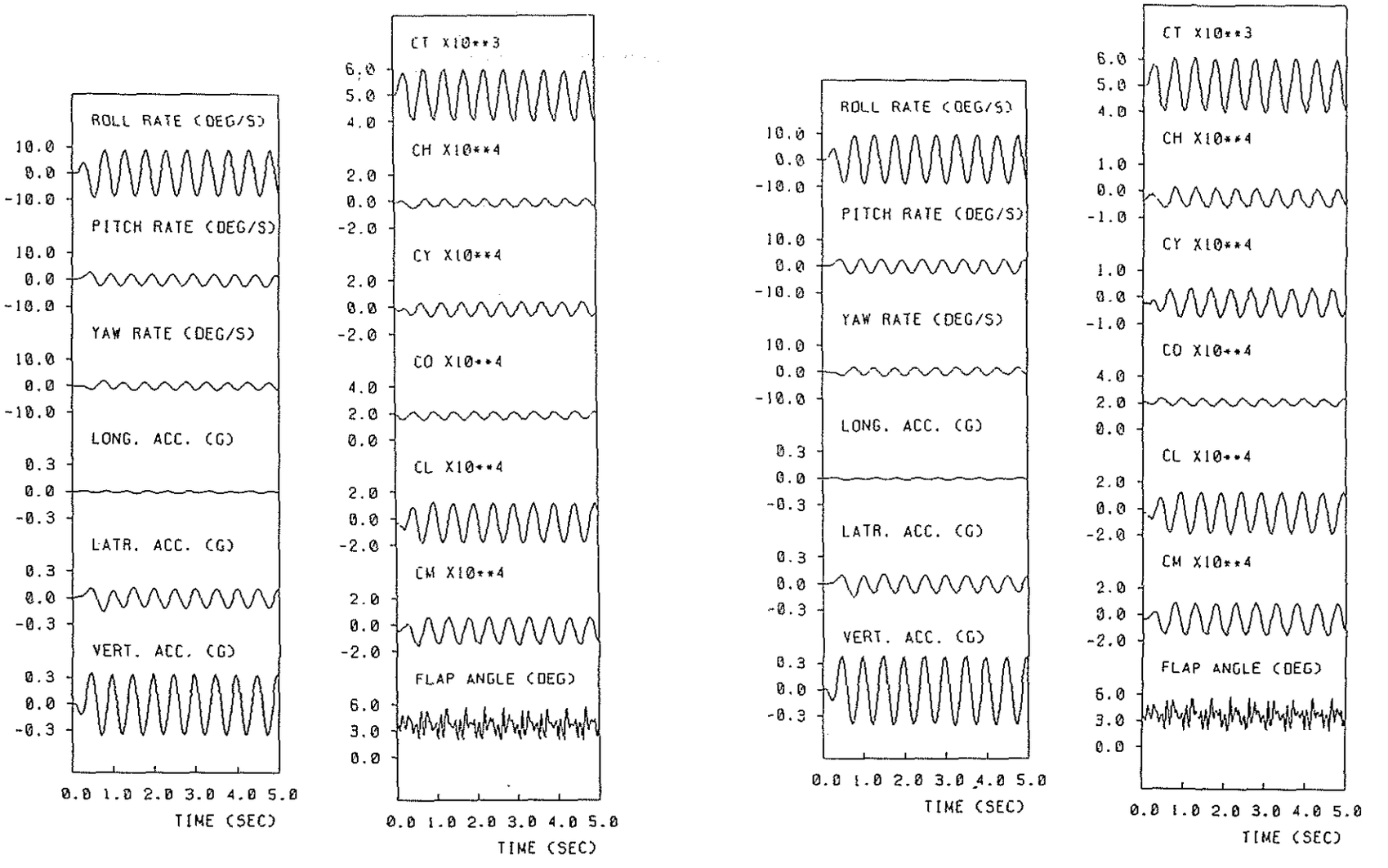

(a) Method of (i) &(b)

(b) Method of (ii)&(b)

Figure 7 Gust responses of the helicopter flying with advance ratio of μ=0.20 for a sinusoidal gust (amplitude of 3m/s and frequency of 2Hz)

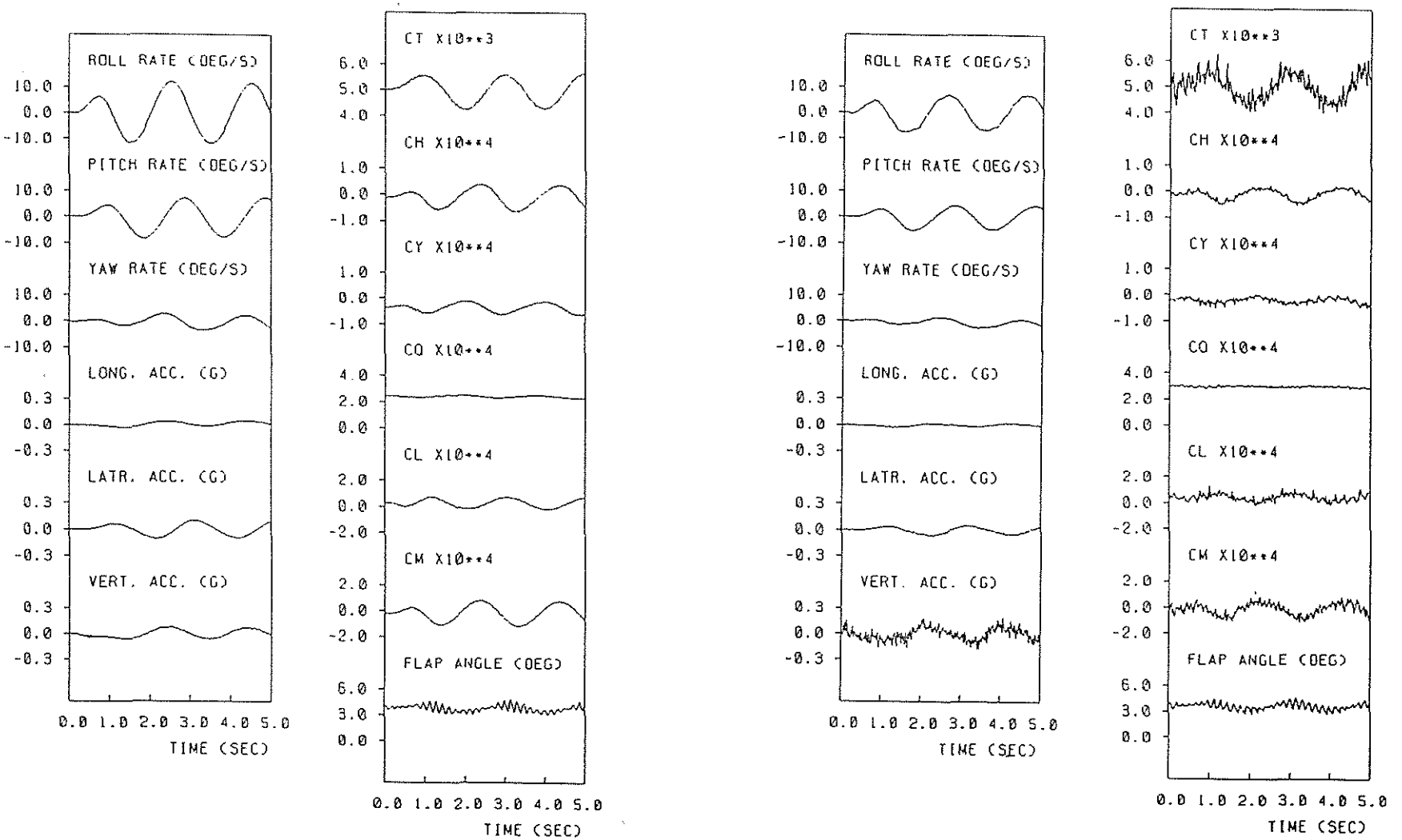

(a) Method of (i) &(b)

(b) Method of (ii)&(b)

Figure 8 Gust responses of the helicopter flying with advance ratio of μ=0.05 for a sinusoidal gust (amplitude of 3m/s and frequency of 0.5Hz)

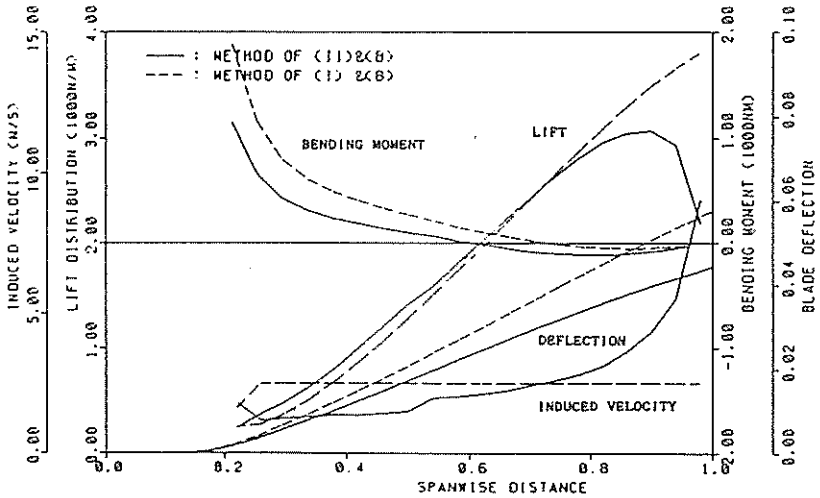

(a) Azimuth angle of 0 deg

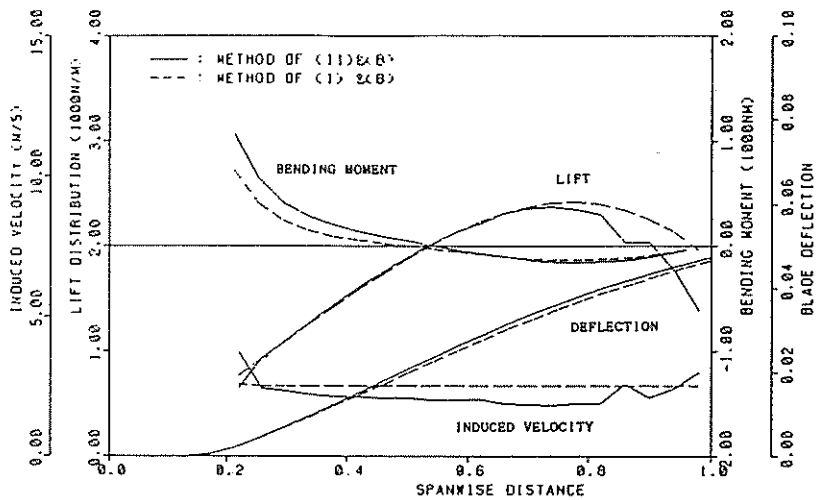

(b) Azimuth angle of 90 deg

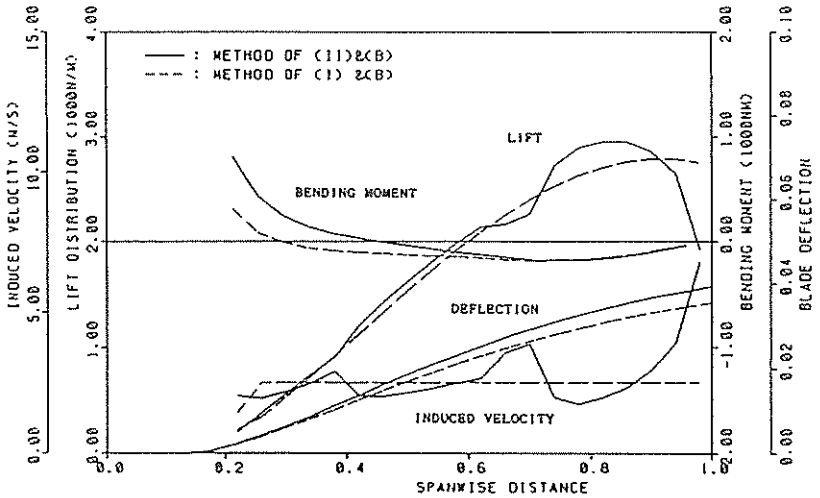

(c) Azimuth angle of 180 deg

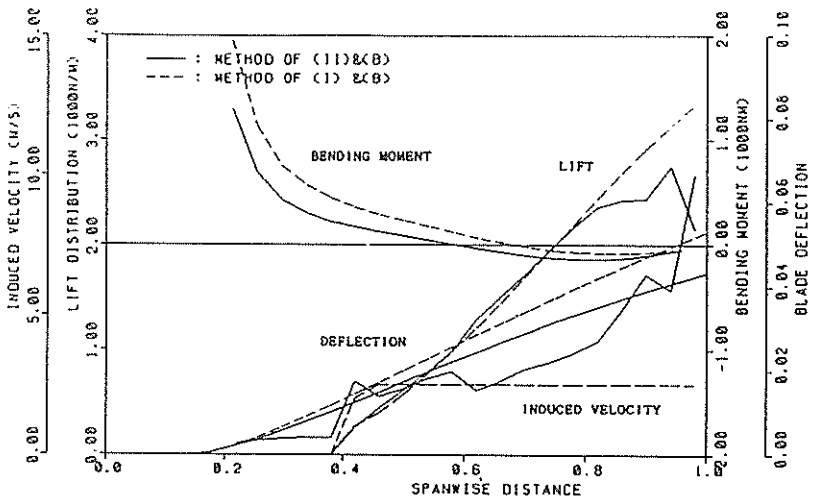

(d) Azimuth angle of 270 deg

Figure 9 Flatwise deflections of blade of the helicopter flying with advance ratio of μ=0.20

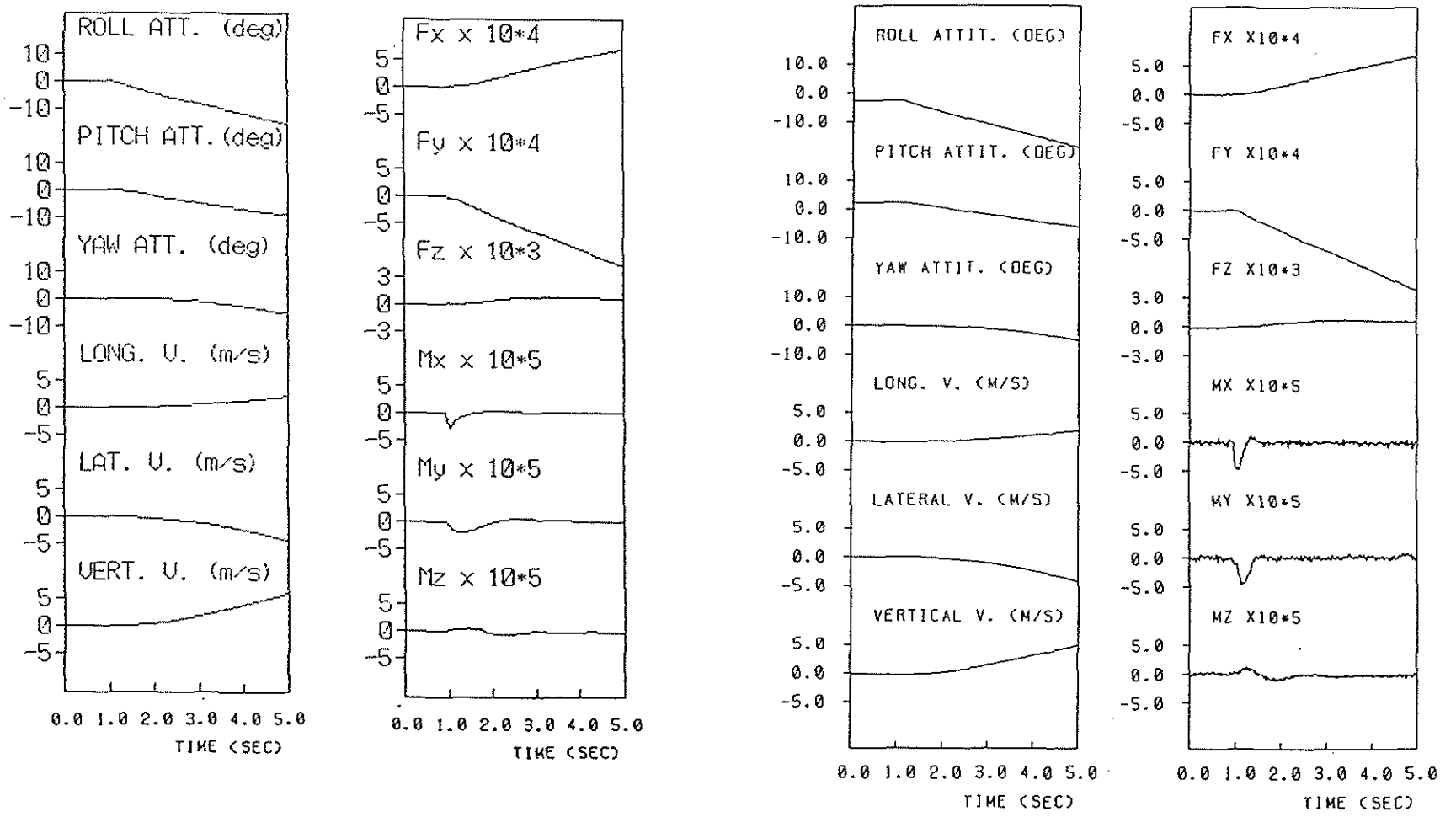

(a) Method of (i) &(a)

(b) Method of (ii)&(b)

Figure 10 Control responses of the helicopter flying with advance ratio of μ=0.20 for a step input ($\Delta\theta$c=0.5°)

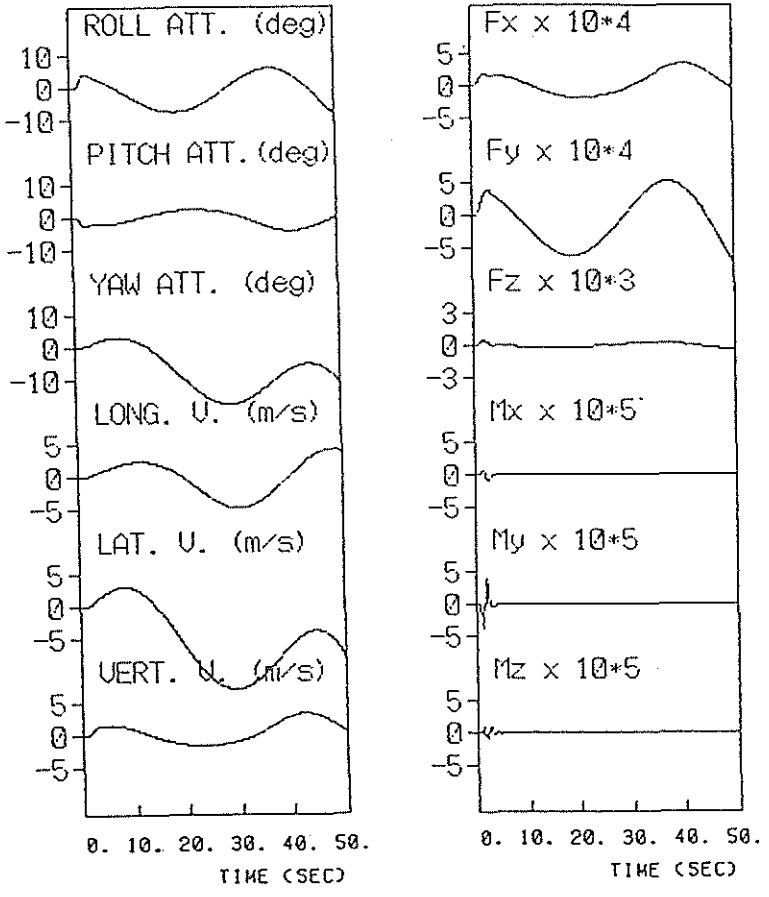

(a) Method of (i) &(a)

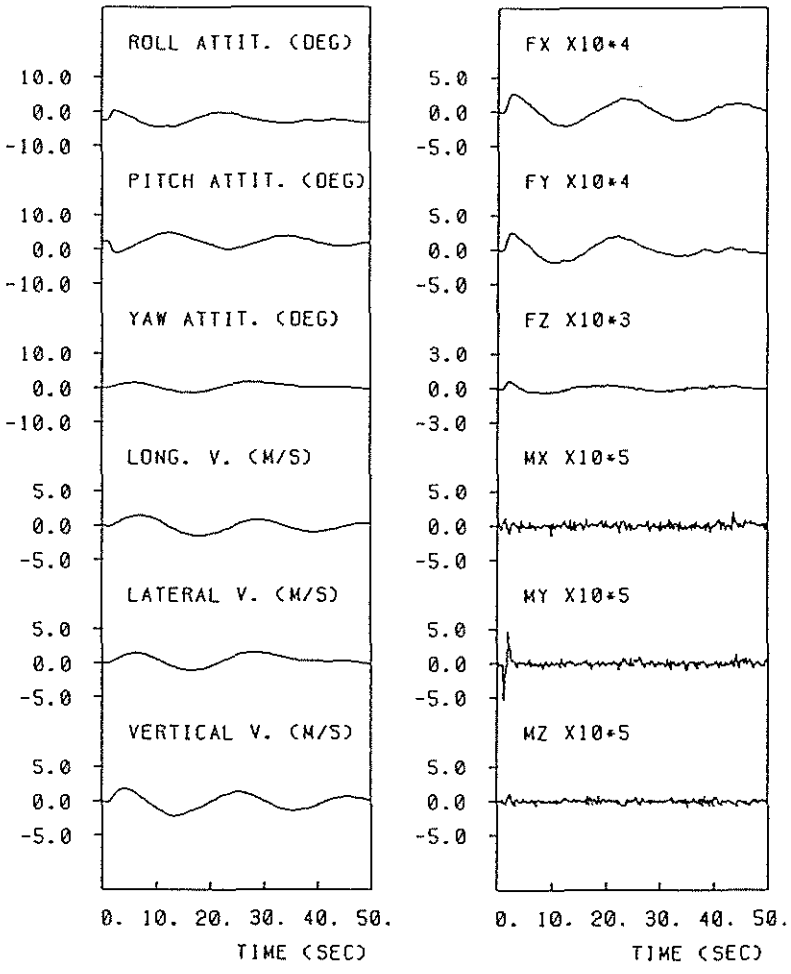

(b) Method of (ii)&(b)

Figure 11 Control responses of the helicopter flying with advance ratio of μ=0.20 for an impulsive input ($\Delta\theta$s=-0.50° and Δt=1s)

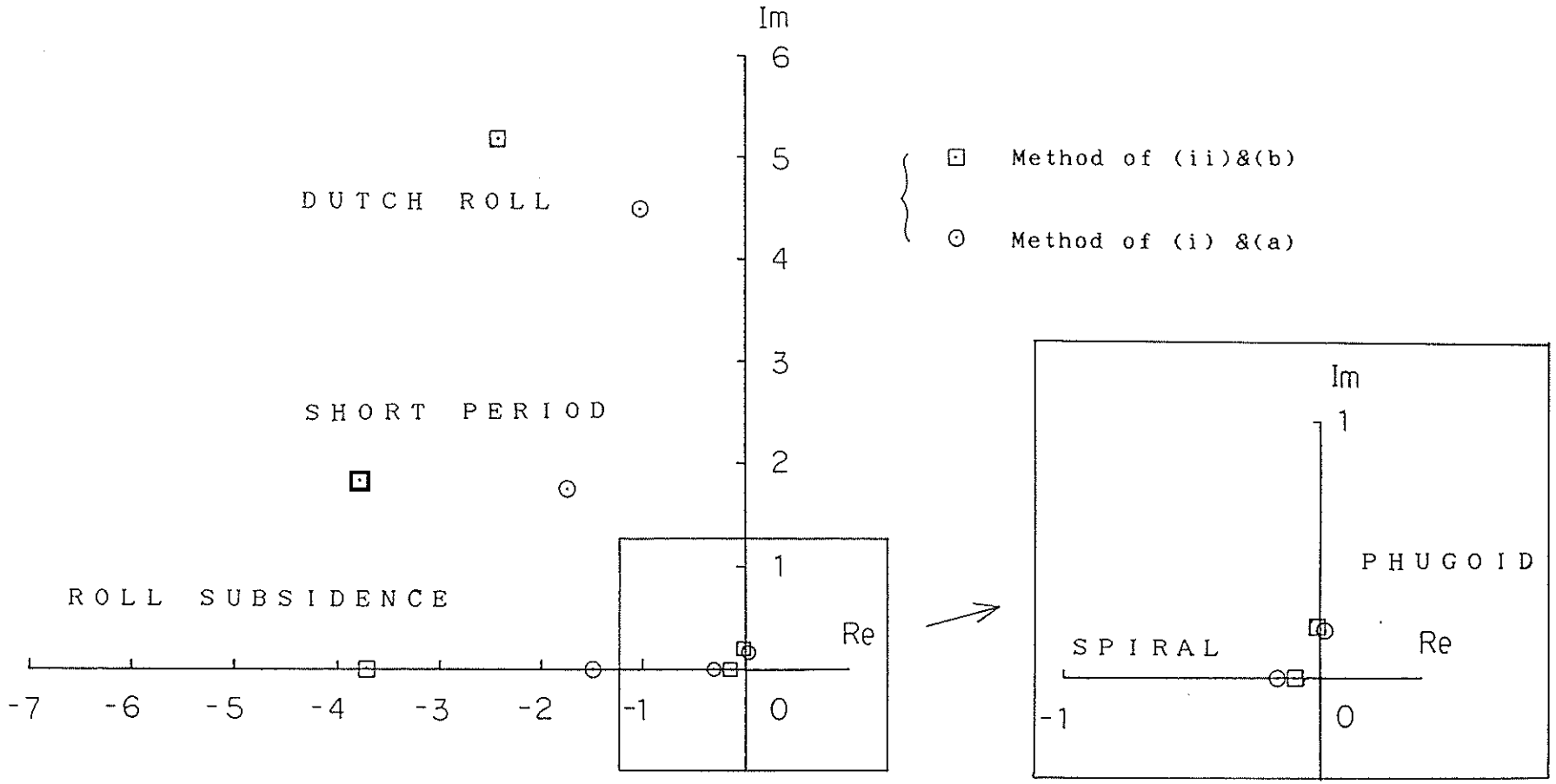

Figure 12 Roots of characteristic equation of the helicopter motion flying with advance ratio of μ=0.20

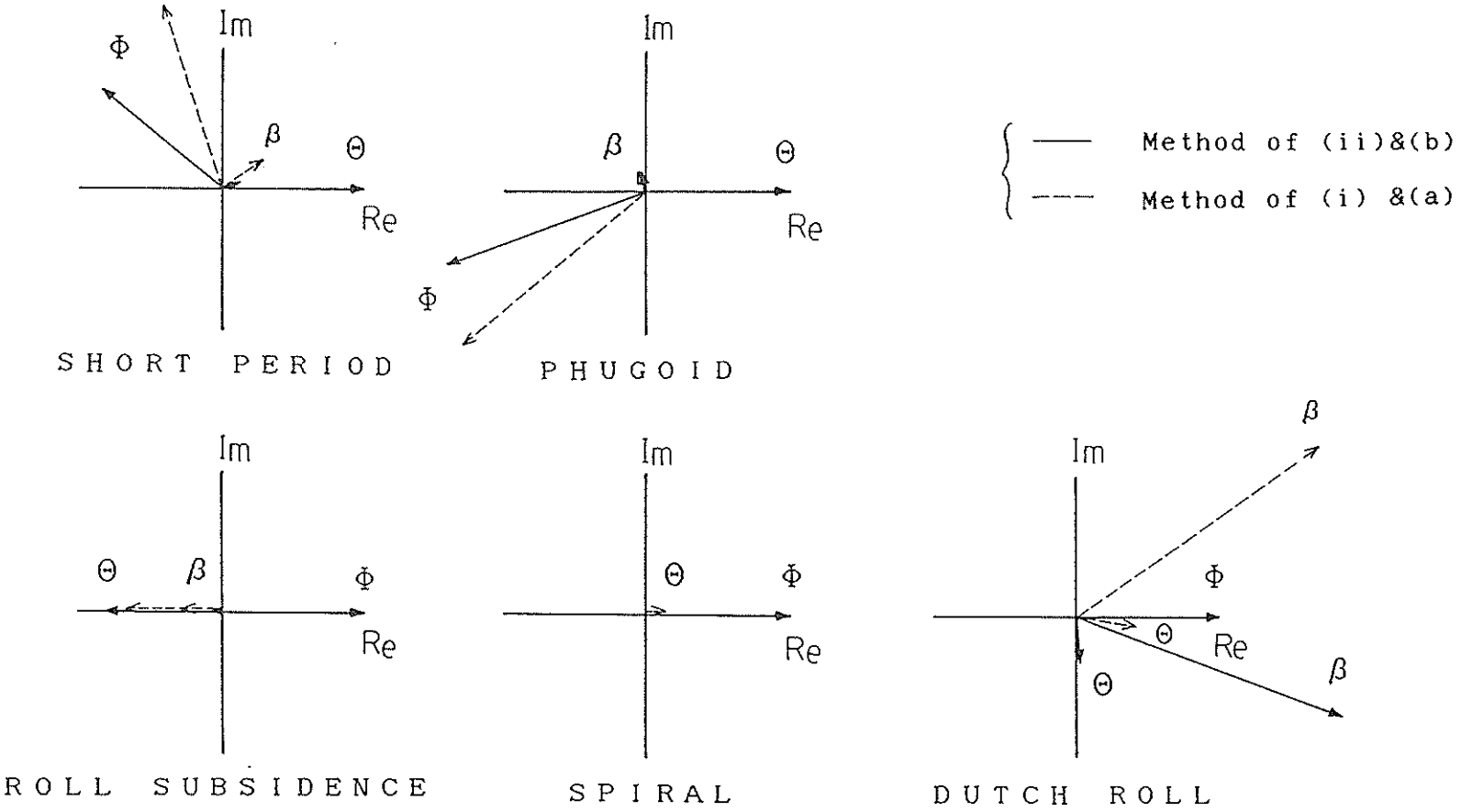

Figure 13 Mode ratios of the helicopter motion flying with advance ratio of μ=0.20